

RESEARCH

Open Access



# Spatial transcriptomics reveals tumor-derived SPP1 induces fibroblast chemotaxis and activation in the hepatocellular carcinoma microenvironment

Wen Tong<sup>1†</sup>, Tianze Wang<sup>2†</sup>, Yi Bai<sup>3</sup>, Xingpeng Yang<sup>4</sup>, Pinsheng Han<sup>2</sup>, Liuyang Zhu<sup>1</sup>, Yamin Zhang<sup>3\*</sup> and Zhongyang Shen<sup>5\*</sup>

## Abstract

**Background** The tumor microenvironment (TME) exerts profound effects on tumor progression and therapeutic efficacy. In hepatocellular carcinoma (HCC), the TME is enriched with cancer-associated fibroblasts (CAFs), which secrete a plethora of cytokines, chemokines, and growth factors that facilitate tumor cell proliferation and invasion. However, the intricate architecture of the TME in HCC, as well as the mechanisms driving interactions between tumor cells and CAFs, remains largely enigmatic.

**Methods** We analyzed 10 spatial transcriptomics and 12 single-cell transcriptomics samples sourced from public databases, complemented by 20 tumor tissue samples from liver cancer patients obtained in a clinical setting.

**Results** Our findings reveal that tumor cells exhibiting high levels of SPP1 are preferentially localized adjacent to hepatic stellate cells (HSCs). The SPP1 secreted by these tumor cells interacts with the CD44 receptor on HSCs, thereby activating the PI3K/AKT signaling pathway, which promotes the differentiation of HSCs into CAFs. Notably, blockade of the CD44 receptor effectively abrogates this interaction. Furthermore, *in vivo* studies demonstrate that silencing SPP1 expression in tumor cells significantly impairs HSC differentiation into CAFs, leading to a reduction in tumor volume and collagen deposition within the tumor stroma.

**Conclusions** This study delineates the SPP1-CD44 signaling axis as a pivotal mechanism underpinning the interaction between tumor cells and CAFs. Targeting this pathway holds potential to mitigate liver fibrosis and offers novel therapeutic perspectives for liver cancer management.

**Keywords** Hepatocellular carcinoma, Cancer-associated fibroblasts, Spatial transcriptomics, Single-cell RNA sequencing, SPP1

<sup>†</sup>Wen Tong and Tianze Wang have contributed equally to this work.

\*Correspondence:

Yamin Zhang  
5020200824@nankai.edu.cn  
Zhongyang Shen  
zhyshtjfc@sina.com

<sup>1</sup>The First Central Clinical School, Tianjin Medical University, Tianjin 300070, China

<sup>2</sup>School of Medicine, Nankai University, Tianjin 300071, China

<sup>3</sup>Department of Hepatobiliary Surgery, Tianjin First Central Hospital, Tianjin 300192, China

<sup>4</sup>Department of General Surgery, First Medical Center of the Chinese PLA General Hospital, Beijing 100853, China

<sup>5</sup>Organ Transplantation Centre, Tianjin First Central Hospital, Tianjin 300192, China



## Introduction

Cancer is a major global public health issue and ranks as the second leading cause of death in the United States [1]. In 2023, the United States is projected to have 1,958,310 new cancer cases and 609,820 cancer-related deaths. Of these, the incidence of Hepatocellular carcinoma (HCC) is gradually increasing [1]. HCC is the fourth leading cause of cancer-related deaths worldwide, and chronic hepatitis B (HBV) virus infection is a major risk factor [2]. Recurrence rates remain high after surgical resection, and patients with unresectable HCC continue to have a poor prognosis and limited treatment options [2]. Recent advancements in medical technology have ushered in a new era of treatment options for various tumor types, including chemotherapeutic agents, targeted therapies, and immunotherapy, providing renewed hope for effective management of these malignancies [3–8]. In this context, the development of specialized nanobiomaterials has emerged as a cornerstone in the therapeutic landscape for cancer patients. These innovative nanobiomaterials facilitate targeted drug delivery systems that not only enhance the therapeutic efficacy of agents but also significantly reduce associated adverse effects [9–11].

More than 80% of HCC cases are characterized by extensive hepatic fibrosis caused by activation, proliferation and accumulation of fibroblasts [12]. A distinctive feature of the HCC tumor microenvironment (TME) is the abundance of cancer-associated fibroblasts (CAFs), which secrete a wide range of cytokines, chemokines, and growth factors that directly or indirectly support cancer cells [12, 13]. According to several recent studies, CAFs play a crucial role in inducing chemoresistance in different tumors, including HCC [14, 15].

Osteobridging protein (OPN) is encoded by the secreted phosphoprotein 1 (SPP1) gene, which has seven exons and a full length of 5 kilobases [16]. Multiple studies have shown that high SPP1 expression is significantly associated with poor prognosis in tumor patients [17–19]. Colorectal cancer-based studies have shown that tumor-specific FAP+ fibroblasts and SPP1+ macrophages are positively correlated, and immunofluorescence staining and spatial transcriptomics validate their tight localization [19]. Moreover, patients with high expression of FAP or SPP1 received less therapeutic benefit in anti-PD-L1 therapy [19]. Pancreatic cancer-based studies have shown that pancreatic cancer cells interact with CAF in the presence of SPP1-CD44-related ligand receptors, and knockdown of SPP1 significantly reduced the stem cell properties of CAF-CM-treated pancreatic cancer cells [17]. The SPP1-CD44 signaling axis enhances cancer stem cell phenotype and promotes aggressive tumor growth in the perivascular ecological niche of glioma [20].

Spatial transcriptomics (ST) combined with single-cell RNA sequencing (scRNA-seq) allows the analysis of gene expression profiles from complete two-dimensional spatial information in tissues. The spatial structure and microenvironmental ecological niche within tumors have been reported to be associated with TME remodeling and tumor metastasis [21]. Multiple single-cell mapping of the HCC tumor microenvironment (TME) based on scRNA-seq technology reveals the heterogeneity of the TME and the diversity of cellular communication that promotes tumor progression [22–24]. Cancer-associated fibroblasts in hepatocellular carcinoma promote tumor growth and metastasis by secreting cytokines [25] and promote immune escape by recruiting monocytes and DCs to induce an immunosuppressive phenotype [26]. Tumor cells and fibroblasts in TME have close spatial proximity, which is necessary for intercellular communication. Blockade or knockdown of SPP1 significantly enhanced PD-1 blockade in a mouse model of hepatocellular carcinoma, which was accompanied by reduced CAF infiltration and increased T-cell toxicity [27].

Our analysis based on spatial transcriptome and single-cell database showed that tumor cells and cancer-associated fibroblasts comprise the tumor microenvironment. Secretion of SPP1 by tumor cells binds to the CD44 receptor on the surface of HSC cells, activating HSC and contributing to their differentiation to CAF. Knockdown of SPP1 from tumor cells inhibited the activation of CAF by CM derived from tumor cells. In vivo experiments showed that knockdown of SPP1 inhibited HSC activation, significantly reduced tumor volume, and significantly reduced collagen deposition in the tumor mesenchyme. Our study provides new perspectives for discovering the mechanism of tumor-mesenchymal interaction and for the treatment of hepatocellular carcinoma.

## Materials and methods

### Clinical samples

Cancer tissues and paracancerous tissues of 20 patients with hepatocellular carcinoma who underwent radical hepatectomy at the Department of Hepatobiliary Surgery of Tianjin First Central Hospital from November 2018 to March 2023 were collected for protein extraction and immunohistochemical staining, and the patients' information was also collected, including gender, age, history of cirrhosis, and TNM stage. All patients had not received any antitumor therapy before surgery. The study was approved by the Ethics Committee of Tianjin First Central Hospital. The clinical information of all patients is shown in Supplementary Table 1.

### Analysis of spatial transcriptome databases

(1): Data source: We searched Pubmed literature for SPP1 related to liver malignancies from 2000 to 2023.

Spatial transcriptome data obtained from the published study (<http://lifeome.net/supp/livercancer-st/data.htm>), in which there are 10 spatial transcriptome samples [21]. (2) After loading the spatial objects with the R package “Seurat,” the SCTransform function normalized the data, followed by clustering for dimensionality reduction using 30 dimensions [28]. Cell type abundance was estimated using marker genes of a certain cell type and AddModuleScore function were used to calculate the cell type enrichment score of a spot. The average expression of SPP1 in each cluster was plotted using the Vlnplot function. (3) Moran’s index analysis: First, the spatial coordinate information for each SPOT, along with SPP1 and fibroblast scoring data, was exported into a spatial transcriptome object. This data was then imported into GeoDa software, where a spatial weight matrix was created and Moran’s index was computed using univariate localized Moran’s I for spatial analysis. Moran’s index is one of the spatial transcriptomics specific statistical indicator of spatial transcriptomics [29, 30]. (4) Correlation analysis between SPP1 expression and cell type enrichment scores: The correlation magnitude and P-value between SPP1 and the 26 cell types were computed with the cor.test function, and a heatmap was generated using the heatmap package. (5) Selection of proximity points in spatial transcriptome samples and analysis of cellular communication: The cluster and cell ID data from the clustered spatial transcriptome were exported from R and imported into Loupe Browser software, where adjacent points in the two clusters were selected manually. These neighboring spots were then imported back into R for analysis. The CellChat package was utilized to analyze and visualize the cellular communication between the spots in the two clusters.

#### Analysis of single-cell databases

Single-cell data were sourced from the GEO database (<https://www.ncbi.nlm.nih.gov/geo/query/acc.cgi?acc=GSE125449>). The data were read into the Seurat package in R, normalized with the SCTransform function, and underwent dimensionality reduction clustering using 15 dimensions and a clustering resolution of 0.2. Cell-type annotations were based on gene markers from Ma L et al. [31]. Cell communication analysis was conducted using the CellChat package.

#### Western blotting

Proteins were extracted from cancer tissues, paraneoplastic tissues, and hepatocellular carcinoma cell lines, and their concentrations were assayed. Electrophoresis samples were prepared and separated using 10% sodium dodecyl sulfate-polyacrylamide gel electrophoresis, then transferred to a polyvinylidene difluoride membrane. The membrane was blocked at room temperature with

5% skimmed milk for 1.5 h and incubated overnight with a primary antibody at 4 °C. After rinsing, a secondary antibody was applied at room temperature for 1.5 h. The membrane was then developed with an ultrasensitive chemiluminescent reagent while protected from light. GAPDH was used as the internal reference, and the experiment was performed three times, with grayscale values analyzed using Image J software. All antibody details for Western blotting are provided in Supplementary Table 2.

#### Cell culture and transfection

Hepatocellular carcinoma cell lines 97 h, huh7, SNU398, LM3, and normal liver cell line THLE-2 were obtained from Shanghai Cell Bank, Chinese Academy of Science. Cells were cultured in DMEM containing 10% fetal bovine serum in an incubator at 37°C with 5% CO<sub>2</sub>. The medium was changed every 2 d. Cells in logarithmic growth phase were taken for subsequent experiments. For cell co-culture experiments, well-grown hepatocellular carcinoma cells were taken, washed three times with PBS, added to DMEM basal medium (serum-free, containing 1% double antibody), cultured for 24 h, and the supernatant was centrifuged at 4 °C, 3000 rpm for 20 min, and after centrifugation the supernatant was slowly aspirated, after which any cells and cellular debris were removed through a 0.2 μm membrane syringe filter, and then added to 10% FBS, which was used as the co-culture conditioned medium (CM) for culturing LX2 cells. For cell transfection experiments, SPP1 (SPP1) shRNA lentiviral were designed and synthesized by Genepharma (Jiangsu, China). Puromycin (Sigma-Aldrich, USA) were used to select stably transduced cells. SPP1 shRNA sequences were as follows: sh-NC:5'-CCTAAGGTTAAGTCGCCCTCG-3'; shSPP1-1:5'-GGCTGAT TCTGGAAGTTCTGA-3'; shSPP1-2: 5'-CTTTACAACA AATACCCAGAT-3'.

#### Immunohistochemical staining

Tissue sections were deparaffinized, hydrated, heated in a microwave oven for 15 min for antigen repair, endogenous peroxidase was removed with 3% H<sub>2</sub>O<sub>2</sub>, and blocked with goat serum. Incubate with primary antibody at 4 °C overnight. Then the secondary antibody was added dropwise, phosphate buffer was washed 3 times, diaminobenzidine colorant was dropped, hematoxylin staining, dehydrated, transparent and sealed. The tissue sections were observed under a light microscope. Scoring was done according to the proportion of positively stained area and the intensity of staining.

#### Immunofluorescence

A sterile coverslip was placed at the bottom of the cell culture plate, and when the cells grew and fused

to 95%~100% on the slide, the slide was removed and washed with phosphate buffer saline (PBS) and then fixed with 4% paraformaldehyde to fix the cell crawler, 0.5% Triton X-100 permeability, 5% BSA block, and then incubated at 4 °C after adding primary antibody. The cells were incubated overnight at 4 °C, washed with PBS and then incubated with fluorescent secondary antibody in a wet box at 37 °C for 1 h. The slices were sealed with a sealing solution containing DAPI antifluorescence quencher, and the cytological morphology images were collected under a fluorescence microscope.

### Xenograft tumor models

Male nude mice were randomly divided into two groups of 5 mice each. Each nude mouse was injected subcutaneously on the right side with  $1 \times 10^6$  97 h cells and  $2 \times 10^6$  LX2 cells. Tumor growth and mouse body weight were monitored every other day. The formula for calculating tumor volume was shown as follows: tumor volume =  $(\text{length} \times \text{width}^2)/2$ . Tumors were obtained 4 weeks after injection. At the end of the experiment, the tumors were excised, photographed, and analyzed by immunohistochemistry and immunoblotting. All animal experiments were approved by the Animal Protection Committee of Tianjin First Central Hospital.

### Sirius red staining

Collagen deposition in tissues was analyzed using a PSR staining kit (Abcam, UK) following the manufacturer's instructions. Tissue sections were deparaffinized, rehydrated, covered with PSR solution for 60 min, rinsed with acetic acid, and dehydrated. Imaging was performed using a Nikon microscope.

### Quantitative RT-PCR

Total RNA was extracted with Trizol reagent (Vazyme Biotech, China). Reverse transcription was performed using ExScript RT-PCR kit (TaKaRa, Japan) according to the protocol. mRNA levels were measured using SYBR Green Master Mix (Vazyme Biotech), with  $\beta$ -actin expression serving as the calibration reference. The  $2^{-\Delta\Delta Ct}$  method was used to calculate the relative expression of target genes. Primer sequences for polymerase chain reaction amplification are provided in Supplementary Table 3.

### Cell viability, wound healing and cell migration assays

Cell viability was evaluated using the Cell Counting Kit 8 (CCK-8) (GLPBIO, USA) following the manufacturer's instructions. For wound healing assay, cells were seeded in 6-well plates and cultured to confluence. Scratch wounds were created with a sterile 200  $\mu$ l pipette tip, washed with phosphate buffer, and cultured with medium containing 10% fetal bovine serum. The

scratches were photographed at 0 and 24 h after scratching, respectively. Migration rate =  $[(0 \text{ h scratch width} - 24 \text{ h scratch width})/0 \text{ h scratch width}] \times 100\%$ . For cell migration experiments, cells were resuspended in serum-free medium. 200  $\mu$ l of serum-free medium containing  $2 \times 10^4$  cells were added to the upper chamber, and then 600  $\mu$ l of medium containing 10% fetal bovine serum was added to the lower chamber. After 48 h of incubation in a cell culture incubator, cells in the upper chamber were fixed with formaldehyde and stained with 0.5% crystal violet. Migrating cells were photographed with an inverted microscope and counted with Image J software. Cell proliferation viability was detected using EDU staining according to the manufacturer's instructions (Elabscience, China). Fluorescent images were imaged and recorded under a fluorescence microscope (Nikon, Japan).

### Statistical analysis

Data are shown as means  $\pm$  standard deviation. Statistical analyses were performed using the GraphPad PRISM (Version 8.0) software. Comparison of groups were conducted using two-sided Student's test and one-way ANOVA.  $P < 0.05$  (two-tailed) was considered statistically significant.

## Results

### Spatial transcriptomics show that elevated SPP1 expression in the HCC TME leads to fibroblast clustering

We performed spatial transcriptome analysis on eight hepatocellular carcinoma samples, using fibroblast markers such as COL1A2, FAP, PDPN, DCN, COL3A1, COL6A1, and COL1A1 to calculate the sample-specific spatial enrichment score (SPOT). Our analysis showed heterogeneity among the samples; three samples (Fig. 1A) exhibited low SPP1 expression and minimal fibroblast presence, while the other five samples (Fig. 1B) displayed high SPP1 expression, increased fibroblast content, and notable structural fibrous tissue in H&E sections. Statistical analysis (Fig. 1C) revealed that SPP1 expression was significantly lower in samples with low fibroblast content compared to those with high content. The high SPP1 group showed considerably greater fibroblast expression than the low SPP1 group (Fig. 1D), indicating a potential role for SPP1 in promoting fibroblast aggregation. Additionally, a positive correlation (correlation coefficient: 0.435) between SPP1 and fibroblast expression was observed across the eight samples (Fig. 1E). Moran's index analysis indicated that in the low SPP1 expression group, both SPP1 and fibroblast expression were spatially dispersed (Moran's index near 0), while in the high SPP1 group, they were clustered (Moran's index near 1) (Fig. 1F, G). Analyzing all eight samples (Fig. 1H and I) revealed a significant difference in the Moran's

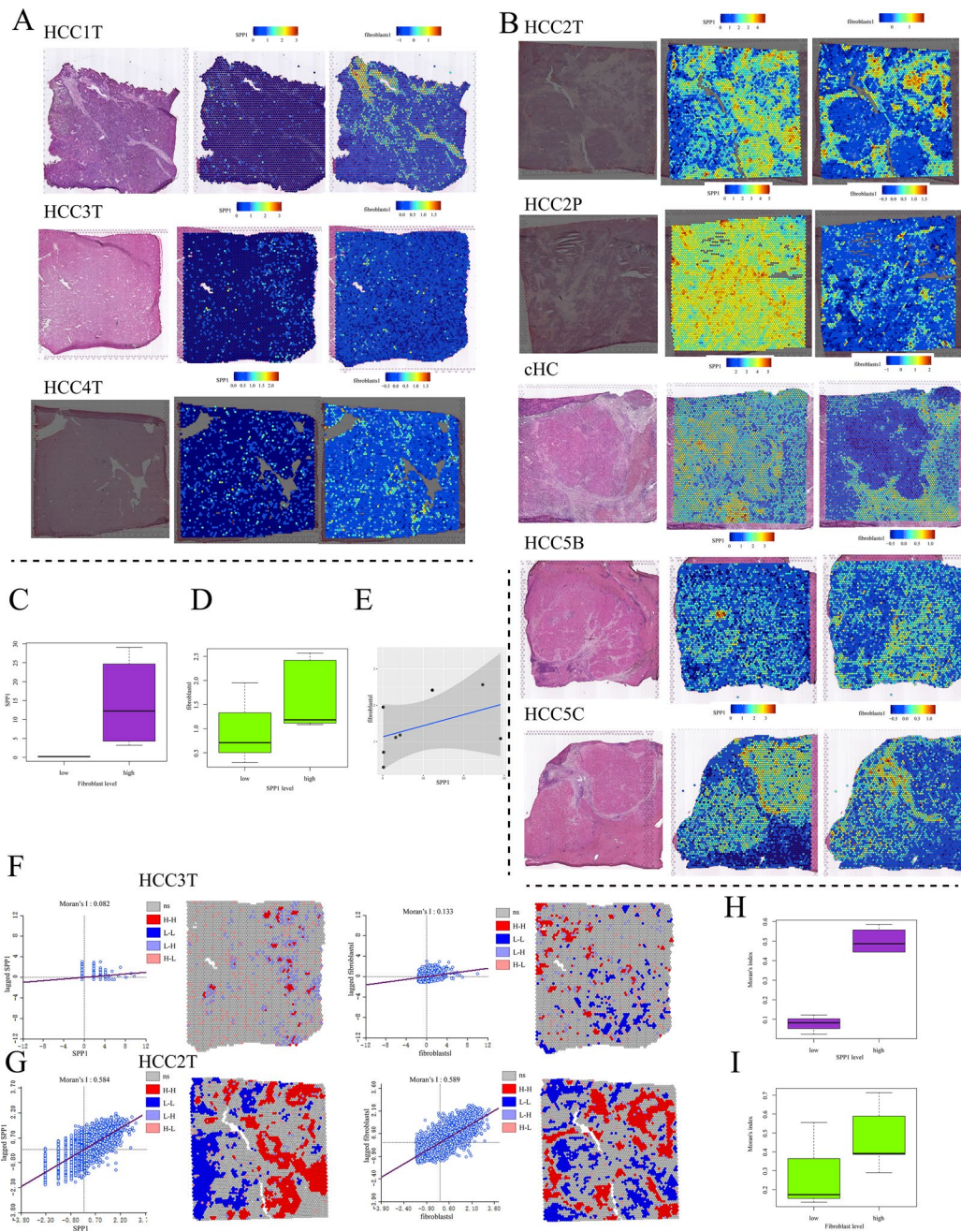


**Fig. 1** Spatial transcriptome-based analysis of the relationship between SPP1 expression and CAF infiltration. **(A)**: Three samples with low SPP1 expression (HCC1T, HCC3T, HCC4T) display their spatial distribution of HE-stained sections, SPP1 levels, and CAF enrichment scores from left to right. **(B)**: Five samples with high SPP1 expression (HCC2T, HCC2P, cHC, HCC5B, HCC5C) illustrate the spatial distribution of HE-stained sections, SPP1 levels, and CAF enrichment scores from left to right. **(C)**: Comparison of average SPP1 expression levels between the low and high SPP1 expression groups. **(D)**: Average expression levels of CAF marker genes in the low and high SPP1 expression groups. **(E)**: Correlation of SPP1 gene expression with CAF marker gene expression in all spatial transcriptomic samples. **(F)**: Local Moran's I index for SPP1 and CAF in the representative sample HCC3T of the low SPP1 expression group, showing Moran scatter plots and LISA cluster maps for SPP1 and CAF from left to right. **(G)**: Local Moran's I index for SPP1 and CAF in the representative sample HCC2T of the high SPP1 expression group, showing Moran scatter plots and LISA cluster maps for SPP1 and CAF from left to right. **(H)**: Average local Moran's I index for SPP1 in the low and high SPP1 expression groups. **(I)**: Average local Moran's I index for CAF in the low and high SPP1 expression groups. \* $p < 0.05$ , \*\* $p < 0.01$ , ns:  $p > 0.05$

index of SPP1 and fibroblasts between the low and high SPP1 expression groups. These findings suggest that the localized expression of SPP1 may drive fibroblast aggregation, potentially contributing to the formation of fibroblastic structures within the hepatocellular carcinoma microenvironment.

### **Spatial transcriptomics indicates cellular interactions between tumor cells and fibroblasts**

Initially, we conducted an analysis of the spatial transcriptome objects utilizing traditional dimensionality reduction clustering methods, as depicted in Fig. 2C and E, followed by cluster annotation. In both spatial transcriptome samples (cHC-1T and HCC-5 C), we observed the highest SPP1 expression in tumor cells, illustrated in Fig. 2A and D. Remarkably, tumor cells exhibiting elevated SPP1 expression were found in close proximity to fibroblasts spatially, as demonstrated in Fig. 2B and E, indicating a potential role for SPP1 secreted by malignant tumors in inducing chemotaxis and aggregation of fibroblasts. Subsequently, employing a non-clustering method, we evaluated the correlation between the enrichment scores of 26 cell types in spots across 10 liver cancer spatial transcriptomes and the expression level of SPP1. Our analysis revealed a strong correlation between SPP1 expression and the scores of malignant tumors in most samples, as highlighted in Fig. 2G, suggesting HCC tumor cells as the primary source of SPP1. Notably, sample HCC5-A displayed a significant positive correlation between SPP1 and tumor cell scores (Fig. 2H).

Furthermore, we investigated the cellular interactions between tumor cell subpopulations with high SPP1 expression and fibroblasts. Notably, in representative samples HCC-2T and HCC-2P, tumor cell subtypes exhibiting high SPP1 expression were found to be spatially adjacent to fibroblasts (Fig. 2I, L). By assessing cellular interactions between tumor cells and fibroblasts in samples HCC-2T and HCC-2P, as shown in Fig. 2J and M, we identified multiple interactions between these cell types. Subsequently, we identified the top 20 ligand-receptor interaction relationships with the most significant interactions, as depicted in Fig. 2K and N, revealing SPP1-associated ligand-receptor interactions between tumor cells and fibroblasts with top-ranked interaction scores. These findings underscore the role of SPP1 signaling in mediating the recruitment of fibroblasts by tumor cells within the hepatocellular carcinoma microenvironment.

### **Single-cell analysis reveals SPP1-CD44 axis between tumor cells and fibroblasts**

In Fig. 3A, the HCC single-cell database (GSE125449) was classified into eight cell types following dimensionality reduction clustering. Figure 3B displays the expression

of marker genes for various cell types; for instance, T cells exhibit high expression levels of CD2, CD3E, CD3D, and CD3G, while B cells show elevated expression of CD79A, SLAMF7, BLNK, and FCRL5. This database comprises 12 samples in total, with the distribution of cell types in each sample illustrated in Fig. 3C. Afterwards, we assessed the SPP1 expression across various cell types, with tumor cells exhibiting the highest levels of SPP1 expression, as illustrated in Fig. 3D and E. This suggests that in the microenvironment of HCC, SPP1 primarily originates from tumor cells. Subsequently, we categorized the 12 samples into SPP1 high-expression and SPP1 low-expression groups based on tumor cell SPP1 levels. Notably, the proportion of fibroblasts in the SPP1 high-expression group was markedly greater than that in the SPP1 low-expression group, as depicted in Fig. 3F. This further implies that elevated SPP1 expression by tumor cells in the HCC microenvironment correlates with increased fibroblast presence. Then, we conducted cellular interaction analysis among various cell populations. In Fig. 3G, numerous interactions were observed between tumor cells and fibroblasts. Subsequently, we delved into the key types of cellular interactions between these two cell types, detailed in Fig. 3H. This figure presented the top 20 most significant interaction pairs between tumor cells and fibroblasts. Notably, among these pairs were two SPP1-associated interactions: SPP1-(ITGAV+ITGB1) and SPP1-CD44, with interaction strengths ranked at 3 and 7, respectively. Additionally, we confirmed the correlation between SPP1 and fibroblast infiltration in the TCGA liver cancer database using the TIMER2.0 platform. Figure 3I illustrates this relationship, showing the correlation between SPP1 and fibroblast infiltration calculated by the EPIC algorithm, yielding a correlation coefficient of 0.311. These findings align with our hypothesis that SPP1 secretion by tumor cells in the liver cancer microenvironment induces fibroblast infiltration.

### **SPP1 expression was significantly upregulated in hepatocellular carcinoma tissues**

To investigate SPP1 mRNA expression in HCC, analysis using the GEPIA database revealed a significant upregulation of SPP1 mRNA in tumor tissues (Fig. 4A). Furthermore, we compared SPP1 expression differences between HCC cell lines and normal liver cell lines. RT-PCR and WB results indicated significantly higher SPP1 expression in tumor cells compared to normal hepatocytes (Fig. 4B, C). To elucidate SPP1 expression in HCC tissues at the protein level, WB and IHC were performed on HCC tissues and corresponding noncancerous liver tissues from the same patient. WB analysis of 5 pairs of HCC samples and matched non-cancerous liver tissues revealed significantly elevated SPP1 levels in HCC tissues (Fig. 4D). Additionally, IHC analysis of 20 pairs of

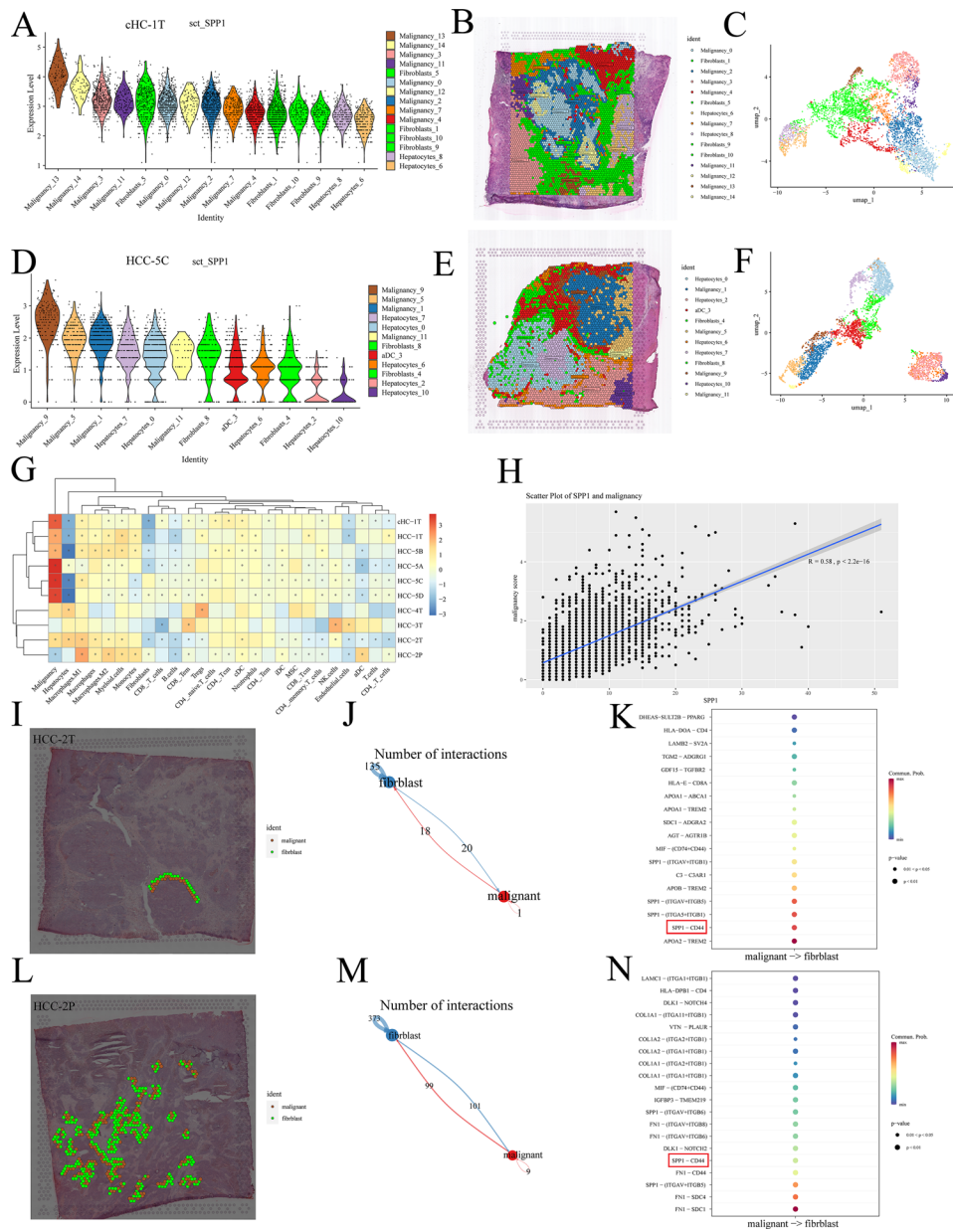


**Fig. 2** SPP1 is primarily secreted by tumor cells and exhibits various ligand-receptor relationships with CAFs. **(A)**: Average SPP1 expression levels of different cell types in the cHC spatial transcriptomic sample. **(B)**: Spatial distribution of different cell types in the cHC spatial transcriptomic sample. **(C)**: Distribution of different cell types in the umap dimensionality reduction space. **(D)**: Average SPP1 expression levels of different cell types in the HCC5C spatial transcriptomic sample. **(E)**: Spatial distribution of different cell types in the HCC5C spatial transcriptomic sample. **(F)**: Distribution of different cell types in the umap dimensionality reduction space. **(G)**: Heatmap showing the correlation between SPP1 expression levels of spots and enrichment scores of 26 cell types in 10 spatial transcriptomic samples. **(H)**: Correlation analysis of SPP1 expression levels and tumor cell scores in HCC5A samples. **(I)**: Spatial distribution between the highest expressing SPP1 malignant tumor subpopulation and CAFs in the HCC2T sample. **(J)**: Cell communication analysis between tumor cells and CAFs selected from Fig. 2I. **(K)**: Bubble chart showing the top 20 significant ligand-receptor interactions between the two cell populations in Fig. 2I. **(L)**: Spatial distribution between the highest expressing SPP1 malignant tumor subpopulation and CAFs in the HCC2P sample. **(M)**: Cell communication analysis between tumor cells and CAFs selected from Fig. 2L. **(N)**: Bubble chart showing the top 20 significant ligand-receptor interactions between the two cell populations in Fig. 2L. \* $p < 0.05$ , \*\* $p < 0.01$ , ns:  $p > 0.05$

clinical samples demonstrated a notable upregulation of SPP1 expression in HCC tissues compared to noncancerous liver tissues (Fig. 4E). As SPP1 is a secreted protein, we assessed its expression in normal and tumor cell line CM using the ELISA method. The results showed a

significantly higher concentration of SPP1 in CM from tumor cell lines compared to normal hepatocyte cell lines (Fig. 4F), suggesting a potential role for SPP1 in HCC development. Analysis of the TCGA-based hepatocellular carcinoma database revealed a significant association

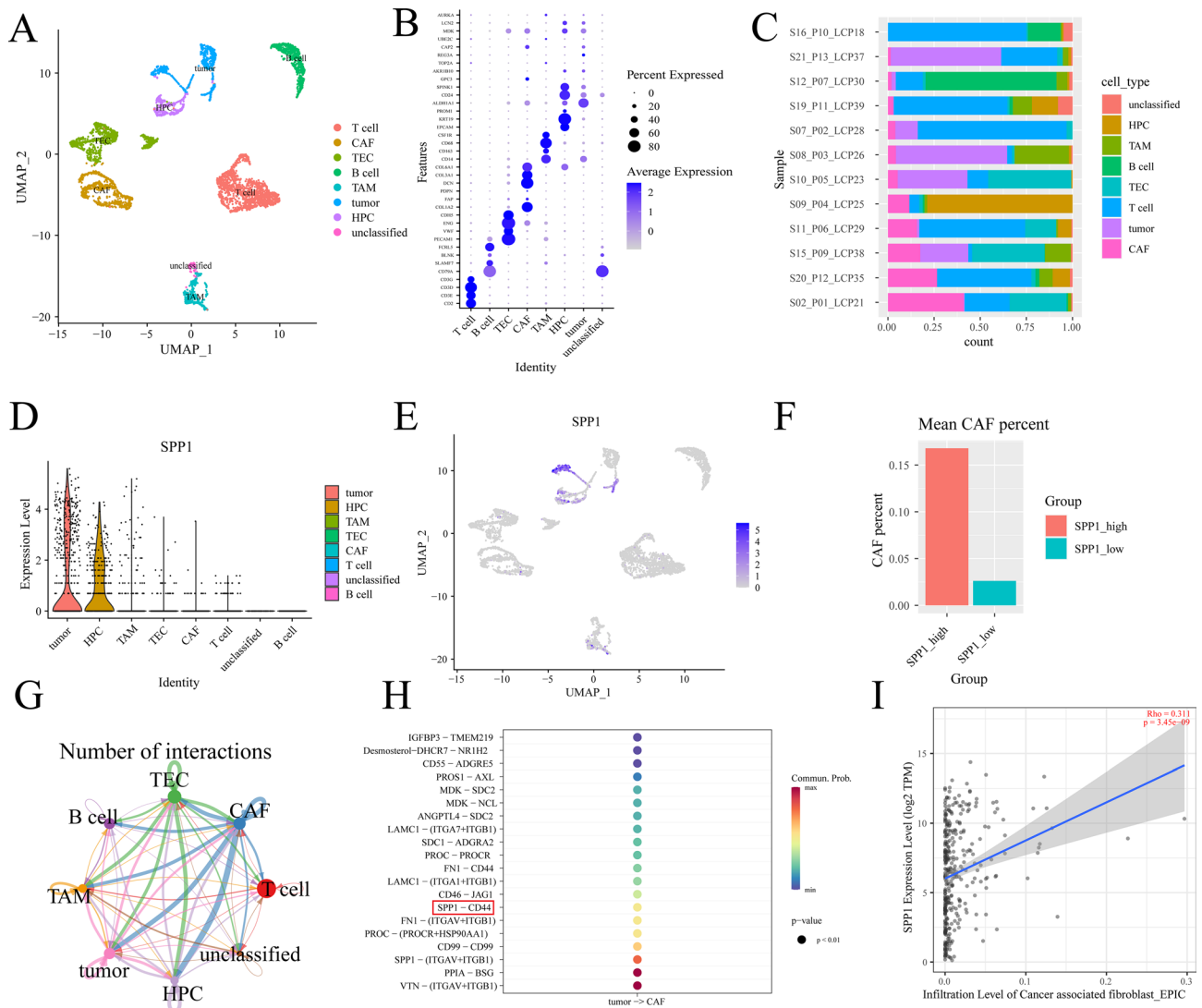


**Fig. 3** Single-cell sequencing analysis of SPP1 expression in relation to CAF infiltration. **(A):** Annotated UMAP clustering map for single-cell objects. **(B):** Identification of classical marker gene expression levels across various cell types. **(C):** Bar chart showing the percentage of cell types within the 12 samples in a single-cell object. **(D):** Violin plots displaying SPP1 expression in different cell types. **(E):** Distribution of SPP1 expression on UMAP projection. **(F):** Mean percentage of fibroblasts in the SPP1 high expression group versus the SPP1 low expression group. **(G):** Cell pairs with ligand-receptor interactions across different cell types. **(H):** The top 20 significant ligand-receptor pairs between tumor cells and fibroblasts. **(I):** EPIC algorithm fitted to the Correlation curves between SPP1 expression (vertical axis) and the degree of fibroblast infiltration (horizontal axis) in the TCGA hepatocellular carcinoma database.  $\rho = 0.311$ ,  $p = 3.45 \times 10^{-9}$ ,  $**p < 0.01$ , ns:  $p > 0.05$

between SPP1 overexpression and poorer overall survival (OS) (Fig. 4G).

### Tumor-derived SPP1 regulates LX2 activation

Multiple studies have demonstrated that SPP1+ macrophages and CAFs situated close to the tumor border form a spatial ecotope that impacts the immune checkpoint blockade's effectiveness [27]. Disruption of TIB structures by blocking SPP1 could enhance the therapeutic efficacy of immune checkpoint blockade in HCC [27]. However, whether SPP1 of HCC cell origin induces trans differentiation of LX2 to CAF has not been clearly

defined. Therefore, we examined whether tumor-derived SPP1 play a role in LX2 activation. We treated LX2 with CM derived from 97 h as well as huh7 (highly expressing SPP1 cells) for 48 h. Western blotting showed that CM derived from 97 h and huh7 cells induced an increase in  $\alpha$ -SMA expression in LX2 cells (Fig. 5A). Next, we successfully down-regulated SPP1 expression in 97 h and huh7 cells using lentivirus, as confirmed by Western blot results (Fig. 5B, C). Since SPP1 is a secreted protein, we utilized an ELISA assay to assess the changes in SPP1 levels in cell supernatants before and after SPP1 knockdown. The results demonstrated a significant reduction in SPP1



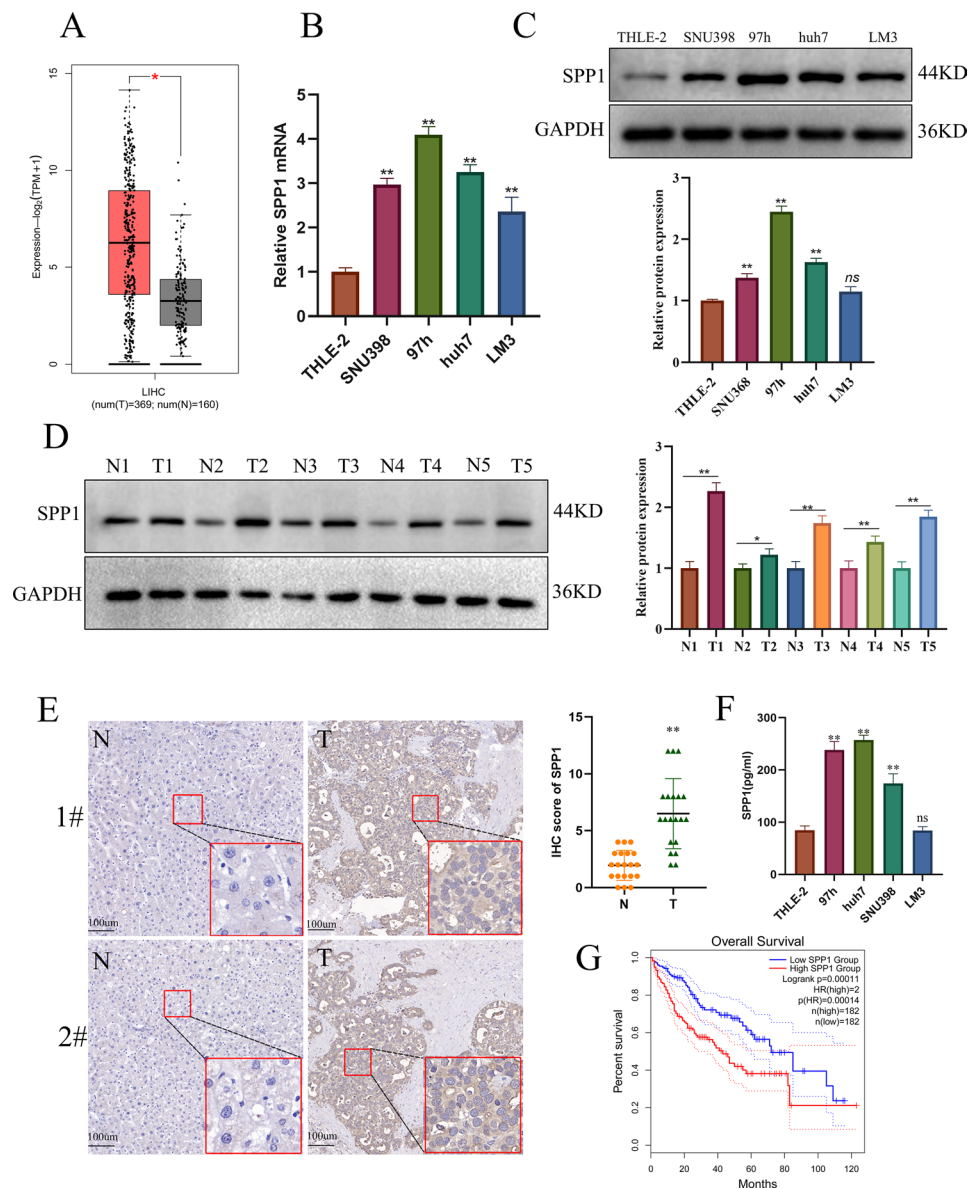


**Fig. 4** Differential expression of SPP1 in normal versus tumor tissues. **(A)**: Analysis of SPP1 expression differences using the TCGA database. **(B)**: RT-PCR revealed expression variations of SPP1 between HCC tumor cells and normal hepatocytes ( $n=3$ ). **(C-D)**: WB assessed SPP1 expression differences in HCC tumor cells versus normal hepatocytes **(C)** and between HCC and normal tissues **(D)** ( $n=3$ ). **(E)**: IHC analyzed SPP1 expression in 20 matched pairs of HCC and normal tissues ( $n=20$ ). **(F)**: ELISA measured differences in OPN content in CM from normal and tumor hepatocytes ( $n=3$ ). **(G)**: TCGA database analysis explored the correlation between SPP1 expression and patient prognosis. \* $p<0.05$ , \*\* $p<0.01$ , ns:  $p>0.05$

in the supernatant following knockdown compared to the control (Supplementary Fig. 1A). Subsequently, we cultured LX2 cells with conditioned media from control 97 h (Ctrl-97 h) and SPP1 knockdown (SPP1-KD1) 97 h, as well as control huh7 (Ctrl-huh7) and SPP1 knockdown (SPP1-KD1) huh7 cells for 48 h (Fig. 5D). Wound healing and transwell assay showed that CM from Ctrl-97 h and Ctrl-huh7 cells increased their migratory ability, whereas CM from SPP1-KD1 97 h and SPP1-KD1 huh7 attenuated this effect (Fig. 5E, Supplementary Fig. 1B, C). Previous studies have shown that LX2 proliferation

and activation produce large amounts of collagen fibers, which generate cirrhosis and promote hepatocellular carcinoma drug resistance, and play an important role in hepatocellular carcinoma progression [32]. Therefore, we examined the proliferative capacity of LX2 after co-culture. EDU and CCK8 experiments showed that CM from Ctrl-97 h and Ctrl-huh7 activated LX2 cells and increased their proliferative capacity compared with the SPP1-KD1 group (Fig. 5E, Supplementary Fig. 1D). In addition, Western blot analysis confirmed that CM from control but not SPP1-KD tumor cells promoted the

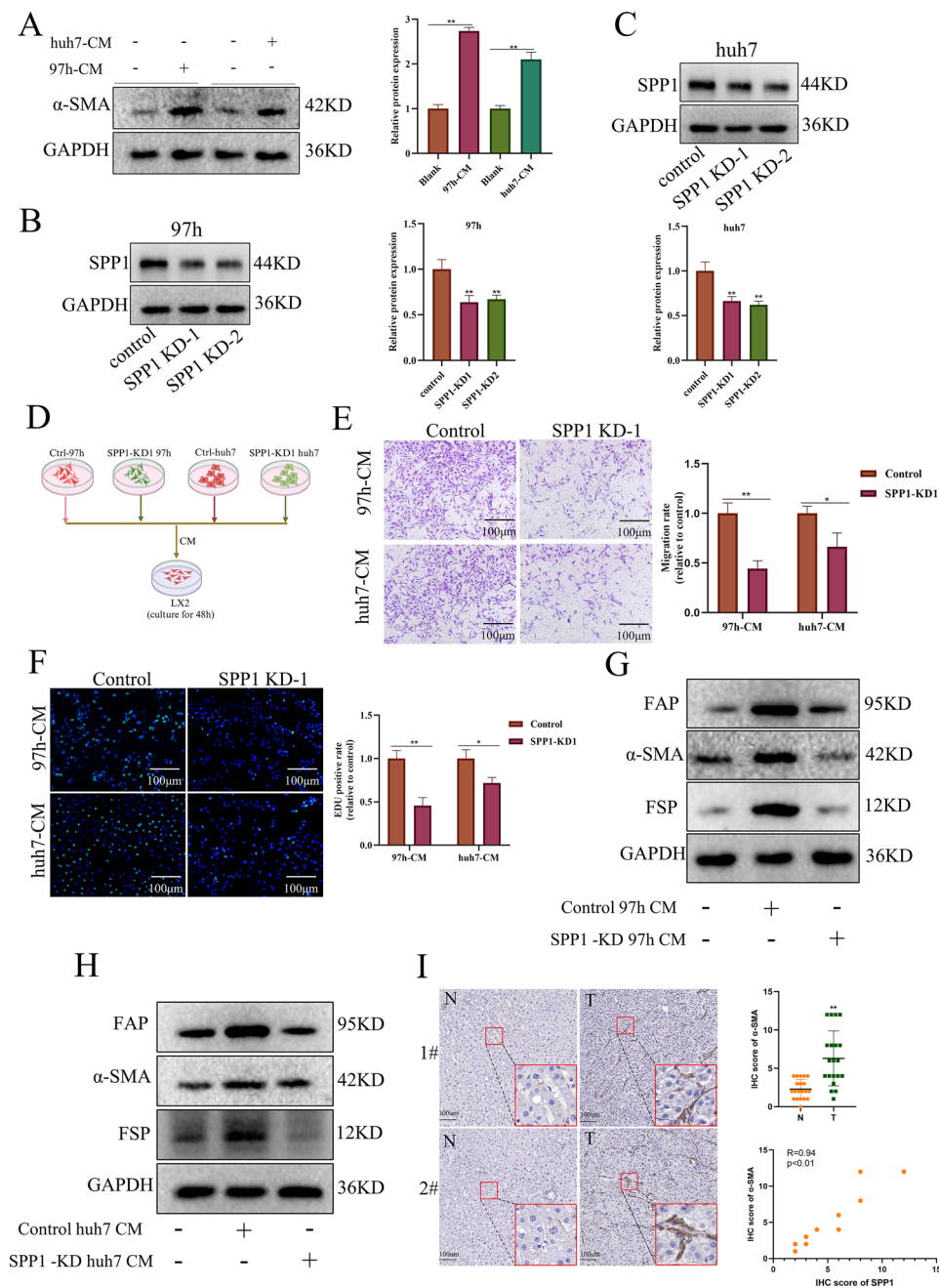


**Fig. 5** HCC cell-derived SPP1 enhanced LX2's migratory ability and upregulated CAF-specific markers. **(A)**: Tumor cell-derived CM stimulated LX2 to express CAF-specific markers ( $n=3$ ). **(B-C)**: 97 h and huh7 cells were infected with SPP1 shRNA lentiviral to silence SPP1 expression, and knockdown efficiency was verified by WB ( $n=3$ ). **(D)**: A flow chart illustrated the culture process of tumor cell CM against LX2. **(E)**: SPP1 from cancer cells increased LX2 migration, demonstrated by a transwell assay after LX2 was cultured with CM from control or SPP1 knockdown tumor cells for 48 h ( $n=3$ ). **(F)**: Cancer cell-derived SPP1 enhanced LX2 proliferation ( $n=3$ ). G-H: HCC cell-derived SPP1 upregulated CAF-specific markers, as validated by CM from 97 h **(G)** and huh7 **(H)** before and after SPP1 knockdown ( $n=3$ ). **(I)**: Immunohistochemistry confirmed SMA expression differences between tumor and paraneoplastic tissues, showing a positive correlation between IHC scores of SPP1 and SMA in tumor tissues ( $n=20$ ). \* $p<0.05$ , \*\* $p<0.01$ , ns:  $p>0.05$

expression of  $\alpha$ -SMA, FAP, and FSP in LX2 cells (Fig. 5G-H, Supplementary Fig. 1E, F). Analysis of spatial transcriptome-based data showed that tumor tissues with high expression of SPP1 also had higher levels of fibroblasts. Therefore, we further used immunohistochemistry to verify the above results in HCC tissue samples.

We found that  $\alpha$ -SMA was significantly highly expressed in HCC tissues relative to paraneoplastic tissues (Fig. 5I). Additionally, correlation analysis of  $\alpha$ -SMA and SPP1 immunohistochemical scores in HCC tissues showed a direct proportionality between SMA and SPP1 expression (Fig. 5I).

### The rOPN reprograms LX2 to CAF

Recruitment and activation of LX2 is a major step in the formation of the CAF population in the TME of HCC [33, 34]. SPP1 is known to be involved in the migration and recruitment of various stromal cell types [18, 27]. Thus, we examined the migratory ability of LX2

after activation by rOPN. Wound healing and transwell assay showed that the motility of LX2 was significantly accelerated 24 h after rOPN activation (Fig. 6A, B). To further clarify the effect of OPN on cell proliferation, we performed EDU experiments. The results showed that OPN significantly promoted LX2 proliferation in

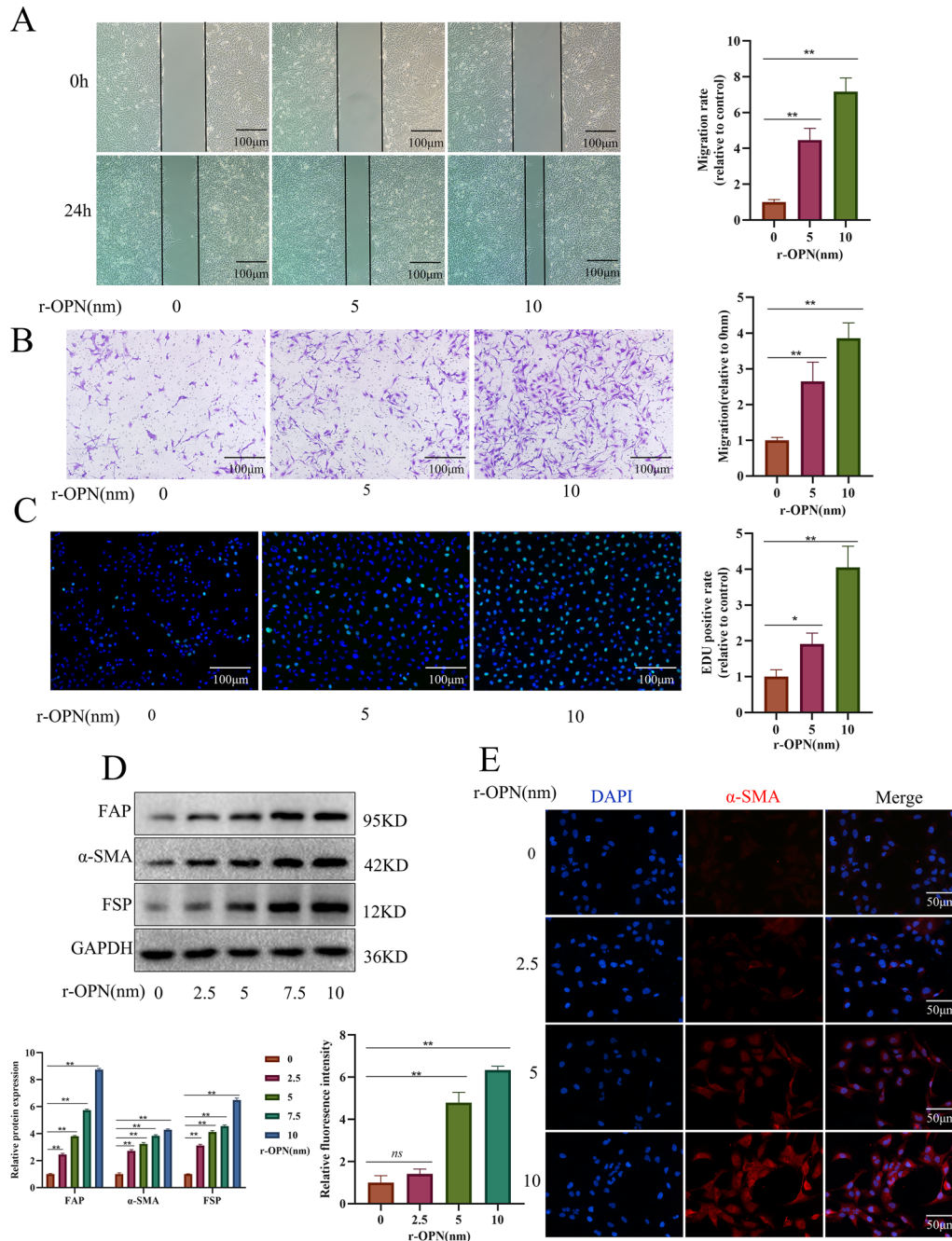


**Fig. 6** r-OPN reprograms LX2 into Tumor-Associated Fibroblasts (CAFs). **(A–B)**: LX2 cells were activated with r-OPN for 24 h, and changes in their migratory capability were assessed using wound healing **(A)** and transwell **(B)** assays ( $n=3$ ). **(C)**: The impact of various concentrations of r-OPN on LX2 proliferation was evaluated via an EDU experiment ( $n=3$ ). **(D)**: Western blot experiments were performed to assess the influence of r-OPN on the expression of CAF markers (FAP, FSP, α-SMA) following treatment of LX2 cells with different concentrations of r-OPN for 24 h ( $n=3$ ). **(E)**: Immunofluorescence experiments were conducted to analyze the effects of r-OPN on the expression of CAF markers (α-SMA) in LX2 cells treated with various concentrations of r-OPN for 24 h ( $n=3$ ). \* $p<0.05$ , \*\* $p<0.01$ , ns:  $p>0.05$

a concentration-dependent manner (Fig. 6C). Next, we attempted to confirm these findings by assessing the expression of CAF-specific markers in LX2 upon rOPN treatment. The results showed that rOPN induced LX2 cells to highly express  $\alpha$ -SMA, FAP, and FSP, which are CAF-specific markers, compared with the control group (Fig. 6D). IF analysis also confirmed that  $\alpha$ -SMA expression in LX2 cells increased significantly with the increase of rOPN treatment concentration. (Fig. 6E).

#### **Tumor-derived SPP1 induces CAF differentiation in an animal model of HCC**

To further confirm the importance of SPP1 in promoting the CAF phenotype in the TME, we established a co-implanted (hepatoma cells and LX2) xenograft HCC animal model (Fig. 7A). The control 97 h and LX2 co-implanted xenograft (CLX) model and the SPP1-KD 97 h and LX2 co-implanted xenograft (SLX) model were constructed by mixing 97 h with LX2 cells (1:2) and then injecting them subcutaneously into nude mice. The data showed that in the CLX model, the weight and volume of the tumors were significantly increased compared to SLX (Fig. 7B-D). RT-PCR and WB results showed that the expression of  $\alpha$ -SMA, FAP, and FSP was reduced at the transcriptional and protein levels in SLX compared to CLX (Fig. 7E, F). The degree of collagen fiber aggregation in the tumor mesenchyme was assessed based on HE and Sirius red staining. Compared with the CLX model, the content of collagen fibers accumulated in the tissues of the SLX model was significantly reduced (Fig. 7G).  $\alpha$ -SMA staining results indicated that the activation of co-implanted LX2 was inhibited in the SLX model, and  $\alpha$ -SMA<sup>+</sup> of CAF cells was significantly reduced (Fig. 7G). In addition, Ki67 staining results showed that the proliferation of CLX tumor cells was enhanced compared with SLX (Fig. 7G). These results indicated that tumor cells secreted SPP1 to promote the conversion of LX2 to CAF, secreted more collagen fibers and promoted tumor tissue growth.

#### **SPP1 promotes LX2 trans differentiation into CAF by activating the PI3K/Akt pathway**

Previous reports have indicated that tumor cell-derived SPP1 binds to the CD44 receptor in fibroblasts, activating the PI3K/Akt pathway and facilitating the transformation of fibroblasts into CAFs [18]. Our spatial transcriptomic data on HCC also confirmed that SPP1 secreted by HCC cells binds to fibroblast CD44. To examine the role of CD44 in SPP1-induced CAF-specific gene expression, we pretreated LX2 cells with an anti-CD44 neutralizing antibody, followed by r-OPN treatment, and analyzed  $\alpha$ -SMA expression. Subsequently, we observed a marked decrease in  $\alpha$ -SMA, FAP and FSP expression in LX2 cells pretreated with the anti-CD44 neutralizing antibody

compared to the group receiving r-OPN alone. This reduction suggests that CD44 is crucial for SPP1-mediated signaling and the subsequent activation of fibrogenic programs in fibroblasts (Fig. 8A). To clarify how SPP1 facilitates the trans differentiation of LX2 into CAFs, we examined SPP1's role in activating the PI3K/Akt pathway. WB analysis revealed that treatment of LX2 with r-OPN for 24 h increased PI3K/Akt phosphorylation (Fig. 8B). However, pre-treating LX2 cells with an anti-CD44 neutralizing antibody before r-OPN administration did not enhance PI3K/Akt phosphorylation (Fig. 8C). Collectively, these results underscore the integral role of SPP1 in driving LX2 trans differentiation into CAFs via the CD44-PI3K/Akt signaling axis, thereby laying the groundwork for future investigations into targeted therapies aimed at modulating this pathway in fibrosis and cancer contexts (Fig. 8D).

#### **Discussion**

Resident fibroblasts in the TME serve as the primary precursor cells of cancer-associated fibroblasts (CAFs) [35]. CAFs represent the predominant stromal cell population within the TME [35, 36], constituting a major component of the tumor stroma. These CAFs play a pivotal role in driving tumor cell proliferation, invasion, and metastasis across various cancer types, including HCC [37, 38]. Recent evidence from multiple studies underscores the critical involvement of CAFs in fostering tumor resistance in diverse malignancies [27, 39–41]. Hepatic stellate cells (HSCs) are notably enriched in precancerous tissues and engage in close interactions with hepatocytes to modulate hepatocellular carcinogenesis by regulating hepatocyte proliferation and apoptosis [21]. Quiescent HSCs secrete hepatocyte growth factors, which confer protective effects on normal hepatocytes, impeding hepatocellular carcinoma development [42]. Conversely, the presence of type I collagen, predominantly found in activated myofibroblast HSCs (mHSCs), promotes tumor cell proliferation and malignant progression by enhancing tissue stiffness, activating TAZ signaling pathways within the liver, and triggering discoidin domain receptor 1 activation [43]. Given the multifaceted roles of CAFs in cancer progression, they emerge as promising targets for therapeutic interventions.

Prior studies have consistently highlighted the upregulation of SPP1 across various tumor types.

Elevated SPP1 levels are notably associated with the transformation of fibroblasts into cancer-associated fibroblasts (CAFs) in breast cancer, leading to the secretion of cytokines that promote tumor cell proliferation and migration [18]. Increased SPP1 expression has also been observed in colorectal cancers, where tumor cells exhibit greater proliferation and drug resistance [19]. In our study of HCC, we found significant SPP1 protein

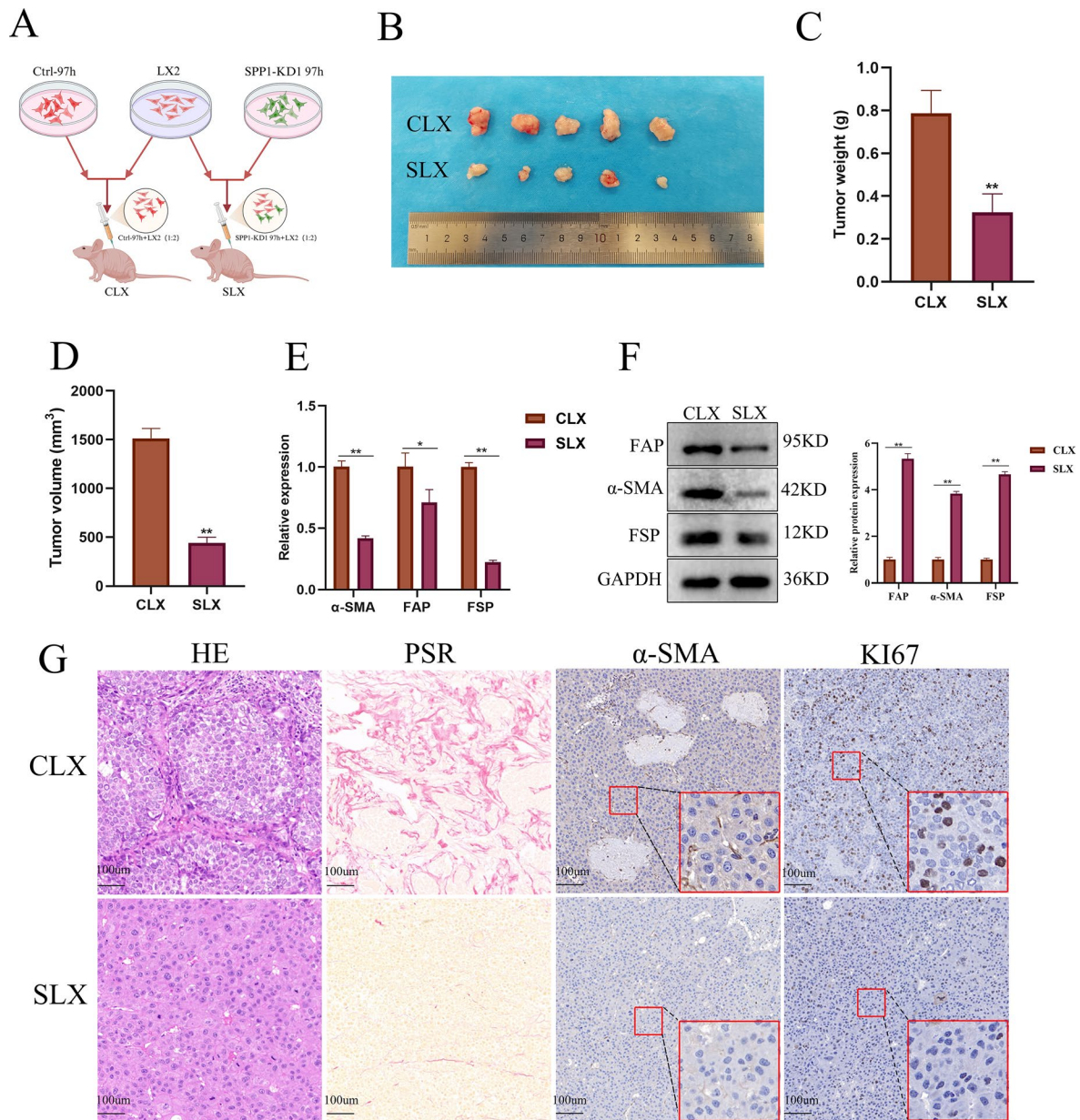


**Fig. 7** Tumor-derived SPP1 induces LX2 differentiation towards CAF in a co-implantation xenograft model. **(A)**: Control 97 h or SPP1-KD1 97 h cells and LX2 cells were co-implanted (1:2 ratio) subcutaneously into 6-week-old male BALB/c nude mice ( $n=5$ ) to construct the Ctrl 97 h and LX2 Co-implantation xenograft (CLX) model and SPP1-KD1 97 h and LX2 co-implanted xenograft (SLX) models. **(B)**: Representative images of tissue samples obtained 3 weeks after the construction of the co-implanted xenograft models are shown. **C-D**: Statistical analyses of tumor weight **(C)** and tumor volume **(D)** between the two groups of samples were conducted ( $n=5$ ). **(E-F)**: RT-PCR **(E)** and WB **(F)** analyses were performed to detect the differences in mRNA and protein expression of CAF markers between CLX and SLX models ( $n=5$ ). **(G)**: HE and Picrosirius red staining were used to identify variations in collagen deposition between CLX and SLX models; Immunohistochemical  $\alpha$ -SMA and KI67 staining were carried out to determine differences in the expression of CAF markers and the proliferative capacity of the tumor cells between CLX and SLX models, respectively ( $n=5$ ). \* $p<0.05$ , \*\* $p<0.01$ , ns:  $p>0.05$

expression across multiple tumor cell lines, with higher SPP1 levels detected in the supernatants of HCC cells compared to normal hepatocytes. Additionally, analysis of clinical samples confirmed elevated SPP1 protein expression in tumor tissues from HCC patients relative to normal tissues. Previous research has highlighted a strong link between high SPP1 expression and poor

clinical outcomes in pancreatic and colorectal cancers [17, 19]. Our findings in HCC similarly indicate that patients with elevated SPP1 expression have significantly shorter overall survival compared to those with lower levels. Together, these results suggest that SPP1 plays a crucial role in tumorigenesis and progression, making it a promising prognostic marker for cancer patients.

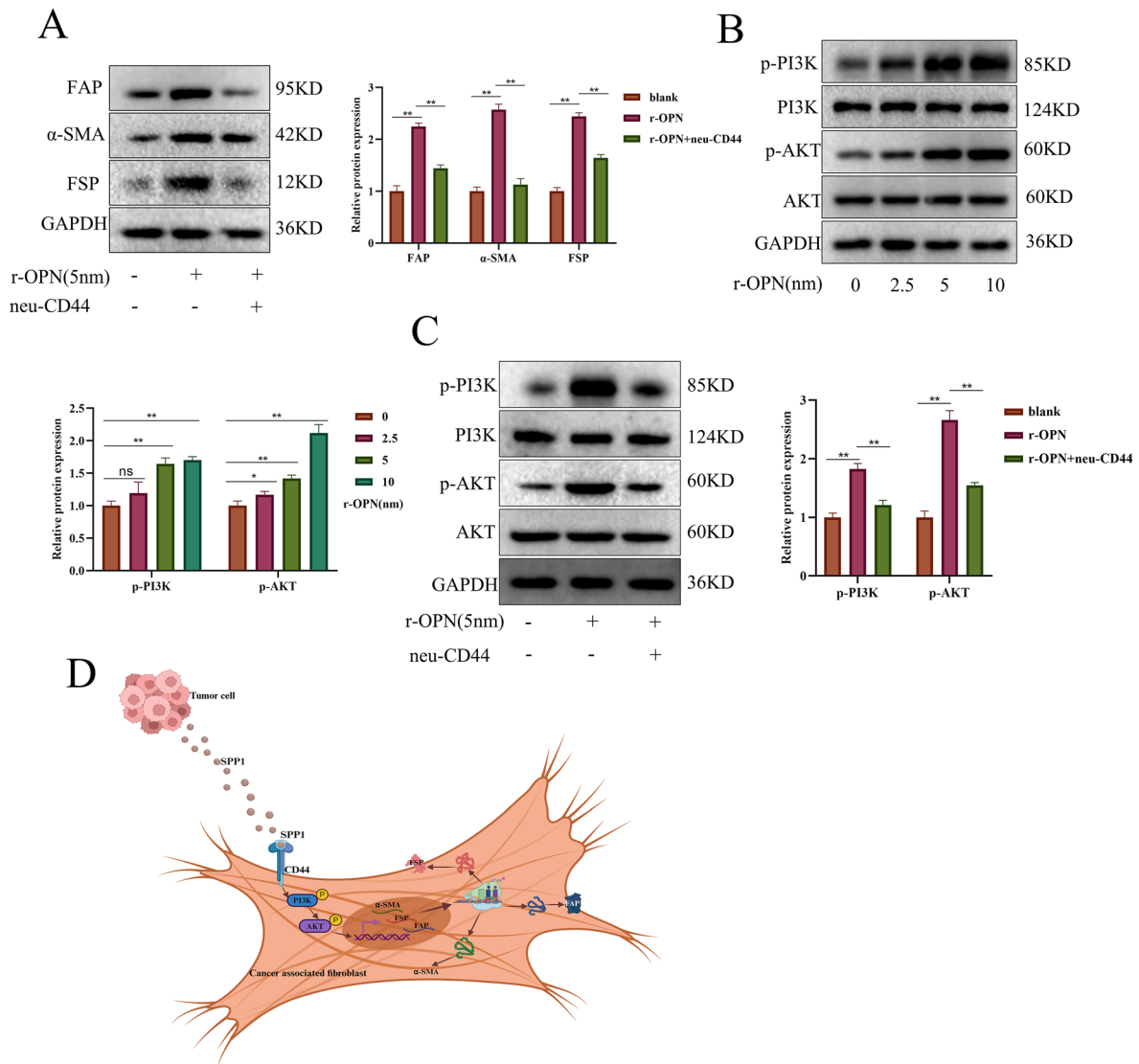


**Fig. 8** Molecular mechanism of SPP1-induced Trans-differentiation of LX2 to Cancer-associated Fibroblasts. **(A):** Blocking the CD44 receptor inhibits the activating effect of recombinant osteopontin (r-OPN) on LX2 cells ( $n=3$ ). **(B):** r-OPN binds to the CD44 receptor, leading to activation of the PI3K/AKT pathway ( $n=3$ ). **(C):** Blocking the CD44 receptor inhibits r-OPN-induced activation of the PI3K/AKT pathway ( $n=3$ ). **(D):** Schematic diagrams illustrate that tumor cell-derived SPP1 binds to the CD44 receptor on LX2 cell membranes, promoting their differentiation into cancer-associated fibroblasts (CAFs) via activation of the PI3K/AKT pathway

Research indicates that secretion of SPP1 by breast cancer cells promotes the transformation of fibroblasts to CAF, thereby promoting the proliferation and migration of CAF cells [18]. In addition, single-cell analysis based on colorectal malignancies also revealed that macrophages and CAFs are spatially close to each other compared to other TME cell types, and that cancer-associated macrophages secrete SPP1 to recruit and activate adjacent fibroblasts, promoting their differentiation to CAFs [19]. In this study, based on single-cell spatial transcriptomic data, we found that in HCC tissues, tumor-associated fibroblasts were spatially located closer to tumor cells, and SPP1 expression was significantly proportional to the degree of fibrosis in the tissues. The results based

on transwell and wound healing assays further indicated that SPP1 secreted by tumor cells or exogenously administered OPN could recruit fibroblasts. Therefore, we hypothesize that liver cancer tumor cells secrete SPP1 to recruit and activate fibroblasts, which in turn secrete more collagen fibers to envelop the tumor tissue.

Studies have shown that fibroblasts release inflammatory cytokines when stimulated by SPP1, which in turn enhance tumor cell proliferation, migration, and EMT transformation [17, 20]. Malignant tumor cells subsequently secrete SPP1 to activate fibroblasts, creating a feedback loop between cancer cells and fibroblasts. Disrupting the interaction between FAP+fibroblasts and SPP1 could enhance the effectiveness of immunotherapy

[19]. Our analysis of HCC spatial and single-cell transcriptome data revealed a ligand-receptor relationship between SPP1 secreted by HCC cells and the CAF cell membrane receptor CD44. Further experiments showed that SPP1 binds to CD44, inducing phosphorylation of PI3K and Akt. Blocking CD44 downregulates the SPP1-induced CAF phenotype. Thus, SPP1 is crucial for maintaining tumor cell stemness through its interaction with CD44. Moreover, our findings indicate that the SPP1-CD44 interaction not only promotes CAF activation but also enhances the secretion of pro-tumorigenic cytokines and growth factors by CAFs. This creates a feedback loop that further sustains the aggressive characteristics of HCC, allowing for tumor progression and metastasis. In vitro assays demonstrated that CAFs stimulated by SPP1 exhibit increased migratory and invasive capabilities, underscoring their role in the tumor microenvironment.

The tumor microenvironment is a dynamic system coordinated by intercellular communication that plays an important role in tumor progression and metastasis [44, 45]. Therefore, it is necessary to study the interaction between tumors and the extracellular matrix. In our study, we first analyzed the differences in SPP1 expression between HCC cells and normal hepatocytes. Then, we found that SPP1 secreted by hepatocellular carcinoma cells recruited hepatic stellate cells and activated the PI3K/AKT signaling pathway to convert HSCs into CAFs by binding to its CD44 receptor. The crosstalk between tumor cells and HSCs further elucidated the molecular mechanism of HCC invasion, explaining the highly invasive nature of hepatocellular carcinoma [46]. In addition, it has been previously reported that SPP1 is elevated to some extent in patients' serum in a variety of cancer types [47]. Our data showed that SPP1 was highly expressed in the supernatants of HCC cell lines compared to normal cells. Also analyzing patient prognosis based on TCGA database found that patients with high expression of SPP1 had poorer prognosis. Therefore, this provides the possibility of serum SPP1 concentration as a diagnostic and prognostic marker for HCC patients.

Previous studies have highlighted the role of SPP1-expressing macrophages and cancer-associated fibroblasts (CAFs) within the hepatocellular carcinoma (HCC) tumor microenvironment, where they collaborate to enhance tumor immune barrier (TIB) formation, thereby limiting the effectiveness of immunotherapy [27]. However, the specific interaction between SPP1 derived from tumor cells and CAFs remains unexplored in HCC. In this study, employing advanced spatial transcriptomics, we present novel findings demonstrating that tumor-derived SPP1 interacts with CAFs, thereby promoting the malignant progression of hepatocellular carcinoma. Remarkably, elevated SPP1 levels are associated with increased fibrosis and a more aggressive tumor

phenotype. Our data showed that HCC tumor cell-derived SPP1 converted HSC into CAFs. Furthermore, in vivo tumorigenic experiments using nude mice demonstrated that SPP1 derived from HCC cells activated the transformation of LX2 cells into CAFs. Analysis of KI67 expression revealed a notable decrease in proliferative capacity and tumor volume in the SPP1 knockdown group compared to the control group. Additionally, tissue samples from the SPP1 knockdown group exhibited reduced activation of tumor-associated HSCs, decreased expression of CAF surface markers, and diminished accumulation of collagen fibers in the tumor stroma. Furthermore, immunohistochemical staining demonstrated reduced levels of  $\alpha$ -SMA and KI67 in tissues associated with SPP1 deficiency, further implicating SPP1 in the modulation of fibroblastic activation within the tumor microenvironment. These results underscore the significance of targeting the SPP1-CAFs interaction as a potential therapeutic strategy in HCC.

Different pharmacologic intervention strategies are usually chosen for the treatment of HCC in clinical practice. For example, chemotherapy, targeted therapy, and immunotherapy. Checkpoint inhibitors have recently made substantial progress in immunotherapy regimens [48]. Angiogenesis inhibitors help in the treatment of advanced hepatocellular carcinoma [49]. However, intervention strategies to block tumor-stromal interactions have been lacking, largely due to limited understanding of the molecular events that crosstalk between tumor cells and their surrounding stromal cells. In this study, we have identified SPP1 and CD44 as mediators of the conversation between HCC and fibroblasts. The development of small molecule inhibitors or monoclonal antibodies against these targets could offer novel adjuvant strategies alongside conventional therapies. Investigating the interplay between SPP1 and CD44 with other pathways involved in HCC could reveal synergistic effects which may further potentiate therapeutic responses.

## Conclusions

The study integrated liver cancer transcriptome data, single-cell sequencing, in vivo and in vitro experiments to propose targeting the SPP1/CD44 axis as a promising therapy for liver cancer, enhancing our understanding of SPP1's role and mechanisms in the disease. The potential of disrupting the SPP1/CD44 axis to halt disease advancement and improve patient outcomes represents a significant step forward in the battle against liver cancer.

## Abbreviations

SPP1	Secreted Phosphoprotein 1
CAF	Cancer-associated Fibroblasts (CAFs)
HCC	Hepatocellular Carcinoma
HSC	Hepatic Stellate Cells
TME	Tumor Microenvironment
ST	Spatial Transcriptomics

scRNA-seq	single-cell RNA sequencing
CM	Conditioned Medium
CLX	Control 97 h and LX2 co-implanted Xenograft (CLX)
SLX	SPP1-KD 97 h and LX2 co-implanted Xenograft

## Supplementary Information

The online version contains supplementary material available at <https://doi.org/10.1186/s12967-024-05613-w>.

Supplementary Material 1  
Supplementary Material 2  
Supplementary Material 3  
Supplementary Material 4

## Acknowledgements

We would like to thank the Lei Chen team for sharing the sequencing data.

## Author contributions

TW, WTZ, ZYM and SZY were involved in designing the study. TW and WTZ contributed to the experimental operation and data analysis. TW drafted the manuscript. BY, YXP, HPS and ZLY participated in revision of the manuscript. All authors read and approved the manuscript. TW and WTZ have contributed equally to this work and share first authorship.

## Funding

This work was supported by the National Natural Science Foundation project (82372194), Tianjin Health Science and Technology Project (TJWJ2021ZD002) and Tianjin Health Science and Technology Project (TJWJ2023MS012).

## Data availability

All raw data related to this study can be obtained by contacting the corresponding author.

## Declarations

### Ethics approval and consent to participate

This study was approved by the Ethics Committee of Tianjin First Central Hospital.

### Consent for publication

All authors agree to publish this study.

### Conflict of interest

The authors have declared that they had no conflict of interest.

Received: 12 April 2024 / Accepted: 13 August 2024

Published online: 12 September 2024

## References

- Siegel RL, Miller KD, Wagle NS, Jemal A. Cancer statistics, 2023. *CA Cancer J Clin.* 2023;73(1):17–48.
- Gordan JD, Kennedy EB, Abou-Alfa GK, et al. Systemic therapy for Advanced Hepatocellular Carcinoma: ASCO Guideline. *J Clin Oncol.* 2020;38(36):4317–45.
- Ali I, Wani WA, Saleem K, Hsieh MF. Anticancer metalodrugs of glutamic acid sulphonamides: in silico, DNA binding, hemolysis and anticancer studies. *RSC Adv.* 2014;4(56):29629–41.
- Ali I, Wani WA, Haque A, Saleem K. Glutamic acid and its derivatives: candidates for rational design of anticancer drugs. *Future Med Chem.* 2013;5(8):961–78.
- Imran Ali HYA, Ghanem A. Enantioselective toxicity and Carcinogenesis. *Curr Pharm Anal.* 2005;1(1):109–25.
- Ding HX, Liu KK, Sakya SM, Flick AC, O'Donnell CJ. Synthetic approaches to the 2011 new drugs. *Bioorg Med Chem.* 2013;21(11):2795–825.
- Ali I, Wani A, Saleem W, Haque K. A. Thalidomide: a banned drug resurged into Future Anticancer Drug. *Curr Drug Therapy.* 2012. 7(1).
- Ali I, Alsehli M, Scotti L, et al. Progress in Polymeric Nano-Medicines for Theranostic Cancer Treatment. *Polym (Basel).* 2020;12(3):598.
- Rosic G. Cancer signaling, cell/gene therapy, diagnosis and role of nanobio-materials. *Adv Biology Earth Sci.* 2024;9:11–34.
- Huseynov E, NOVEL NANOMATERIALS FOR HEPATOBIILIARY DISEASES, TREATMENT AND FUTURE PERSPECTIVES. *Adv Biology Earth Sci.* 2024;9:81–91.
- Baran A, Baran MF, Keskin C, Kandemir SI, Valiyeva M, Mehraliyeva S, et al. Ecofriendly/Rapid Synthesis of Silver Nanoparticles Using Extract of Waste Parts of Artichoke (*Cynara scolymus* L.) and evaluation of their cytotoxic and antibacterial activities. *J Nanomaterials/Journal Nanomaterials/Journal Nanomaterials.* 2021;2021(1):2270472.
- Affo S, Yu LX, Schwabe RF. The role of Cancer-Associated fibroblasts and fibrosis in Liver Cancer. *Annu Rev Pathol.* 2017;12:153–86.
- Yin Z, Dong C, Jiang K, et al. Heterogeneity of cancer-associated fibroblasts and roles in the progression, prognosis, and therapy of hepatocellular carcinoma. *J Hematol Oncol.* 2019;12(1):101.
- Gao Q, Zhu H, Dong L, et al. Integrated Proteogenomic characterization of HBV-Related Hepatocellular Carcinoma. *Cell.* 2019;179(2):561–e57722.
- Ruiz de Galarreta M, Bresnahan E, Molina-Sánchez P, et al.  $\beta$ -Catenin activation promotes Immune escape and resistance to Anti-PD-1 therapy in Hepatocellular Carcinoma. *Cancer Discov.* 2019;9(8):1124–41.
- Song Z, Chen W, Athavale D, et al. Osteopontin takes Center Stage in Chronic Liver Disease. *Hepatology.* 2021;73(4):1594–608.
- Nallasamy P, Nimmakayala RK, Karmakar S, et al. Pancreatic tumor microenvironment factor promotes Cancer Stemness via SPP1-CD44 Axis. *Gastroenterology.* 2021;161(6):1998–e20137.
- Butti R, Nimma R, Kundu G, et al. Tumor-derived osteopontin drives the resident fibroblast to myofibroblast differentiation through Twist1 to promote breast cancer progression. *Oncogene.* 2021;40(11):2002–17.
- Qi J, Sun H, Zhang Y, et al. Single-cell and spatial analysis reveal interaction of FAP(+) fibroblasts and SPP1(+) macrophages in colorectal cancer. *Nat Commun.* 2022;13(1):1742.
- Pietras A, Katz AM, Ekström EJ, et al. Osteopontin-CD44 signaling in the glioma perivascular niche enhances cancer stem cell phenotypes and promotes aggressive tumor growth. *Cell Stem Cell.* 2014;14(3):357–69.
- Wu R, Guo W, Qiu X, et al. Comprehensive analysis of spatial architecture in primary liver cancer. *Sci Adv.* 2021;7(51):eabg3750.
- Aizarani N, Saviano A, Sagar, et al. A human liver cell atlas reveals heterogeneity and epithelial progenitors. *Nature.* 2019;572(7768):199–204.
- Sharma A, Seow J, Dutertre CA, et al. Onco-fetal reprogramming of endothelial cells drives immunosuppressive macrophages in Hepatocellular Carcinoma. *Cell.* 2020;183(2):377–e39421.
- Song G, Shi Y, Zhang M, et al. Global immune characterization of HBV/HCV-related hepatocellular carcinoma identifies macrophage and T-cell subsets associated with disease progression. *Cell Discov.* 2020;6(1):90.
- Sun L, Wang Y, Wang L, et al. Resolvin D1 prevents epithelial-mesenchymal transition and reduces the stemness features of hepatocellular carcinoma by inhibiting paracrine of cancer-associated fibroblast-derived COMP. *J Exp Clin Cancer Res.* 2019;38(1):170.
- Deng Y, Cheng J, Fu B, et al. Hepatic carcinoma-associated fibroblasts enhance immune suppression by facilitating the generation of myeloid-derived suppressor cells. *Oncogene.* 2017;36(8):1090–101.
- Liu Y, Xun Z, Ma K, et al. Identification of a tumour immune barrier in the HCC microenvironment that determines the efficacy of immunotherapy. *J Hepatol.* 2023;78(4):770–82.
- Hao Y, Hao S, Andersen-Nissen E, Mauck WM 3rd, Zheng S, Butler A, et al. Integrated analysis of multimodal single-cell data. *Cell.* 2021;184(13):3573–e8729.
- Jackson MC, Huang L, Xie Q, Tiwari RC. A modified version of Moran's I. *Int J Health Geogr.* 2010;9:33.
- Li Z, Wang T, Liu P, Huang Y. SpatialDM for rapid identification of spatially co-expressed ligand-receptor and revealing cell-cell communication patterns. *Nat Commun.* 2023;14(1):3995.
- Ma L, Hernandez MO, Zhao Y, et al. Tumor Cell Biodiversity drives Microenvironmental Reprogramming in Liver Cancer. *Cancer Cell.* 2019;36(4):418–e4306.
- Liu B, Zhou Z, Jin Y, et al. Hepatic stellate cell activation and senescence induced by intrahepatic microbiota disturbances drive progression of liver cirrhosis toward hepatocellular carcinoma. *J Immunother Cancer.* 2022;10(1):e003069.



33. Avgustinova A, Iravani M, Robertson D, et al. Tumour cell-derived Wnt7a recruits and activates fibroblasts to promote tumour aggressiveness. *Nat Commun*. 2016;7:10305.
34. Caligiuri G, Tuveson DA. Activated fibroblasts in cancer: perspectives and challenges. *Cancer Cell*. 2023;41(3):434–49.
35. Lavie D, Ben-Shmuel A, Erez N, Scherz-Shouval R. Cancer-associated fibroblasts in the single-cell era. *Nat Cancer*. 2022;3(7):793–807.
36. Kalluri R. The biology and function of fibroblasts in cancer. *Nat Rev Cancer*. 2016;16(9):582–98.
37. Costa A, Kieffer Y, Scholer-Dahirel A, et al. Fibroblast heterogeneity and immunosuppressive environment in human breast Cancer. *Cancer Cell*. 2018;33(3):463–e47910.
38. Galbo PM Jr, Zang X, Zheng D. Molecular features of Cancer-associated fibroblast subtypes and their implication on Cancer Pathogenesis, Prognosis, and Immunotherapy Resistance. *Clin Cancer Res*. 2021;27(9):2636–47.
39. Qu X, Liu B, Wang L, et al. Loss of cancer-associated fibroblast-derived exosomal DACT3-AS1 promotes malignant transformation and ferroptosis-mediated oxaliplatin resistance in gastric cancer. *Drug Resist Updat*. 2023;68:100936.
40. Wang H, Li N, Liu Q, et al. Antiandrogen treatment induces stromal cell reprogramming to promote castration resistance in prostate cancer. *Cancer Cell*. 2023;41(7):1345–e13629.
41. Qi R, Bai Y, Li K, et al. Cancer-associated fibroblasts suppress ferroptosis and induce gemcitabine resistance in pancreatic cancer cells by secreting exosome-derived ACSL4-targeting miRNAs. *Drug Resist Updat*. 2023;68:100960.
42. Akk?z H. Emerging role of Cancer-Associated fibroblasts in progression and Treatment of Hepatocellular Carcinoma. *Int J Mol Sci*. 2023;24(4):3941.
43. Eun JW, Yoon JH, Ahn HR, et al. Cancer-associated fibroblast-derived secreted phosphoprotein 1 contributes to resistance of hepatocellular carcinoma to sorafenib and lenvatinib. *Cancer Commun (Lond)*. 2023;43(4):455–79.
44. Donne R, Lujambio A. The liver cancer immune microenvironment: therapeutic implications for hepatocellular carcinoma. *Hepatology*. 2023;77(5):1773–96.
45. Li XY, Shen Y, Zhang L, Guo X, Wu J. Understanding initiation and progression of hepatocellular carcinoma through single cell sequencing. *Biochim Biophys Acta Rev Cancer*. 2022;1877(3):188720.
46. Song M, He J, Pan QZ, et al. Cancer-Associated fibroblast-mediated Cellular Crosstalk supports Hepatocellular Carcinoma Progression. *Hepatology*. 2021;73(5):1717–35.
47. Yan Z, Hu X, Tang B, Deng F. Role of osteopontin in cancer development and treatment. *Heliyon*. 2023;9(10):e21055.
48. Tison A, Garaud S, Chiche L, Cornec D, Kostine M. Immune-checkpoint inhibitor use in patients with cancer and pre-existing autoimmune diseases. *Nat Rev Rheumatol*. 2022;18(11):641–56.
49. Bejarano L, Jord?jo M, Joyce JA. Therapeutic targeting of the Tumor Microenvironment. *Cancer Discov*. 2021;11(4):933–59.

### Publisher's note

Springer Nature remains neutral with regard to jurisdictional claims in published maps and institutional affiliations.